Pigmentary TiO2: a challenge for its use as photocatalyst in NOx air purification

Pigmentary TiO_2: a challenge for its use as photocatalyst in NOx air purification

Claudia L. Bianchi[a], Carlo Pirola[a], Federico Galli[a], Giuseppina Cerrato[b], Sara Morandi[b], Valentino Capucci[c].

[a] *Dipartimento di Chimica, Università degli Studi di Milano, via Golgi 19, 20133 Milano, Italy, and Consorzio INSTM, via Giusti 9, 50121 Firenze, Italy.*

[b] *Dipartimento di Chimica and NIS, Center of Excellence, Università di Torino, Via P. Giuria 7, 10125 Torino, Italy, and Consorzio INSTM, 50121 Firenze, Italy.*

[c] *Graniti Fiandre SpA, Via Radici Nord 112, 42014 Castellarano, Italy.*

Corresponding author:

Claudia L. Bianchi

phone: +39 0250314253

Fax: +39 0250314300

e-mail: claudia.bianchi@unimi.it

postal address: Dipartimento di Chimica

Università degli Studi di Milano

Via Golgi 19, 20133 Milano, Italy.

Abstract

The photocatalytic degradation of NO_x in the gas phase was investigated comparing several commercial TiO_2 sold as pigmentary-powders and characterized by crystallite sizes ranging from nano to micrometer dimensions. In particular the photocatalytic activity of the micro-sized sample was evaluated in comparison with the well-known activity of the nano-sized samples, being these last photocatalysts potentially dangerous due to the risk towards the human safety. The studied samples were precisely chosen among different commercially available products on the basis of the following features: pure anatase, uncoated surface, undoped material, not sold as photocatalytic materials. All samples reveal good photoactivity in the photodegradation of NO_x in gas phase with an evident superiority of the nano-sized sample. However, the gap of activity between nano and micro-sized samples tends to be canceled when the starting NO_x concentration was reduced and fixed from 1000 to 200 ppb, a precise amount that is the first alert threshold for NO_x in air (World Health Organization). A proper kinetic model, based on the Langmuir-Hinshelwood mechanism and on the hypothesis of irreversible adsorption of the products on the catalysts surface, has been developed and discussed.

Keywords: photocatalysis, micro-sized TiO_2, pigmentary materials, NOx degradation, kinetic model.

Graphical abstract

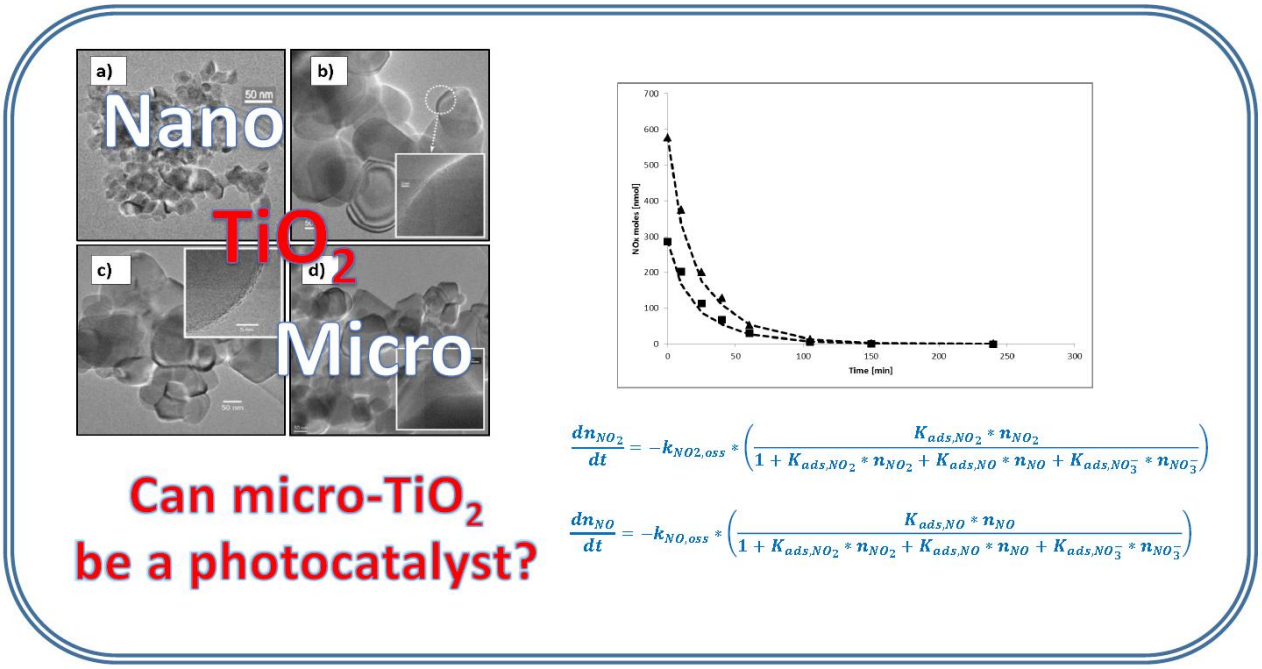

1. Introduction

Titania is a very well-known and well-researched material due to the stability of its chemical structure, biocompatibility, physical, optical, and electrical properties. Its photocatalytic properties have been utilized in various environmental applications to remove contaminants from both water and air [1].

However, titanium dioxide is also the most widely used white pigment because of its brightness and very high refractive index, in which only a few other materials surpass it. More than 5 million tons of pigmentary TiO_2 are consumed annually worldwide, and this number is expected to increase as consumption continues to rise. When deposited as a thin film, its refractive index and color make it an excellent reflective optical coating for dielectric mirrors and some gemstones like "mystic fire topaz". TiO_2 is also an effective opacifier in powder form, where it is employed as a pigment to provide whiteness and opacity to products such as paints, coatings, plastics, papers, inks, foods, medicines (i.e. pills and tablets) as well as most toothpastes.

Heterogeneous photocatalysis is a process in which photochemistry and catalysis are operating together. It implies that both light and catalyst are necessary to bring out the chemical reaction. UV light illumination over a semiconductor like TiO_2 produces electrons and holes. The valence band holes are powerful oxidants, while the conduction band electrons are good reductants [2]. The world of photocatalysis always focused the attention on ultra-small semiconductor particles that has become one of the fastest growing research areas in physical chemistry. In fact, materials reduced to the nanoscale can suddenly show very different properties compared to what they exhibit on a microscale because of both surface and volume effects [3].

Nano-sized TiO_2 is extremely efficient towards the degradation of pollutants both in air and in water and also possesses enhanced photoredox chemistry [4]. However, in the last period, a growing uncertainty raised upon the use of nano-sized powders due to possible risks towards the human safety as our tissues are not able to recognize crystallites of so small sizes which can penetrate into the human body either from skin or directly by breathing [5].

To avoid this, a couple of investigations on the possibility to use TiO_2 characterized by larger-sized crystallites began a few years ago demonstrating the possibility to employ such a material for the photodegradation of pollutant molecules in both gas- and liquid phase [6, 7]. Parallel to these, the performances of two commercial micro-sized TiO_2 were compared to that of two nano-sized samples in the photocatalytic degradation of acetone, acetaldehyde and toluene in gas phase, evidencing good results for all systems [8].

In the present work, the photoactivity towards the degradation of NO_x in the gas phase was evaluated comparing several commercial pigmentary-powdered TiO_2 as both nano-sized and micro-sized samples. In all cases, samples were chosen with the following features: pure anatase, uncoated surface, undoped material, not sold as photocatalytic materials

Samples were fully characterized investigating textural, structural, morphological and surface properties. NOx degradation results were compared with those obtained by P25 by Evonik, a commercial TiO_2 sample specifically sold as photocatalyst and always used as reference material in photocatalysis.

All pigmentary samples show good photoactivity towards the degradation of NO_x in gas phase. As expected P25 exhibits the highest efficiency towards the photodegradation of NO_x especially at high pollutant amount (1000 ppb), but this gap drastically decreases when tests were performed using lower amount of pollutant such as 200 ppb, a value

however often far from the real level of pollution of the most polluted cities worldwide, but identified as the alert threshold for human safety by World Health Organization [9] and reported in the EU directive on air quality [10].

These experimental data have been interpreted through the development of a suitable mathematical model able to represent the different step of the mechanism of degradation of NO_x by the photocatalytic process. The proposed model is based on the two following main assumptions: 1) the Langmuir-Hinshelwood (LH) mechanism for the adsorption and further photocatalytic degradation of the reactants and 2) an irreversible adsorption of the products on the TiO_2 surface [11].

2. Materials and Methods

Five commercially available pigmentary-powdered TiO_2 were chosen with the following features: pure anatase, uncoated surface, un-doped material, not sold as photocatalytic material. These samples will be labelled as A, B, C, D, E. Moreover P25 by Evonik was used as photocatalytic reference material. The main characteristics of all these samples are reported in Table 1.

2.1. Sample characterization

The specific surface area (SSA) of all samples was determined by N_2 adsorption/desorption experiments at 77 K (BET method) using a Sorptometer instrument (Costech Mod. 1042).

The crystalline nature of the samples was investigated by X-ray diffraction (XRD) using a PW3830/3020 X'Pert diffractometer from PANalytical working Bragg-Brentano, using the

Cu $K_{\alpha 1}$ radiation (λ = 1.5406 Å). The calculation of the crystallite size was performed by employing the Scherrer equation:

$$D = 0.9 \cdot \lambda / (\beta_{hkl} \cdot \cos\theta_{hkl})$$

where D is the crystallite size, λ is the X-ray wavelength of radiation for CuKα, β_{hkl} is the full-width at half maximum (FWHM) at (hkl) peak and θ_{hkl} is the diffraction angle.

The morphology of the catalysts was inspected by means of high resolution electron transmission microscopy (HR-TEM) using a JEOL 3010-UHR instrument (acceleration potential: 300 kV; LaB_6 filament). Samples were "dry" dispersed on lacey carbon Cu grids.

X-ray photoelectron spectra (XPS) were taken in an M-probe apparatus (Surface Science Instruments). The source was monochromatic Al Kα radiation (1486.6 eV).

For the band-gap determinations, diffuse reflectance spectra of the powders were collected on a UV-Vis scanning spectrophotometer (PerkinElmer, Lambda 35), which was equipped with a diffuse reflectance accessory. A TiO_2 thin film was placed in the sample holder on integrated sphere for the reflectance measurements. A "total white" PerkinElmer reference material was used as the reference. Data were elaborated using the Kubelka-Munk function [12]:

$$F(R) = (1- R)^2/2\ R$$

R = reflectance of the powder. The band-gap values were determined by performing the first derivative of the Kubelka-Munk function:

$$dF(R)/d\lambda$$

λ = wavelength of the incident radiation. The energy of the radiation at which the first derivative $dF(R)/d\lambda$ shows the maximum was taken as an estimation of the band-gap values.

Finally, the study of the surface hydroxyl species by means of in situ FT-IR spectroscopy has been carried out. Absorption/transmission IR spectra have been obtained on a Perkin-Elmer FT-IR System 2000 spectrophotometer equipped with a Hg-Cd-Te cryo-detector, working in the range of wavenumbers 7200-580 cm^{-1} at a resolution of 2 cm^{-1} (number of scans ~20). For IR analysis powder catalyst has been compressed in self-supporting disc (of about 10 mg cm^{-2}) and placed in a homemade quartz cell, equipped with KBr windows, connected to a conventional high-vacuum line (UHV). Spectra were recorded at room temperature (RT) on the samples in air and after prolonged outgassing at RT.

2.2. Photocatalytic tests

The photocatalytic activity of the samples was tested in NO_x degradation. Their efficiency was monitored using a setup precisely described elsewhere [13] operating in static condition. Photocatalytic degradations were conducted in a Pyrex glass cylindrical reactor with an effective volume of 20 L. The amount of catalyst (in the form of powder deposited from 2-propanol slurry on flat glass plate, size 20 x 2 cm, as described in [14]) used in the tests was 0.05 g. The gaseous mixture in the reactor was obtained by mixing NO_2 (0.6% in nitrogen) with air humidified at 40%. It is important to underline that we start from an inlet gas of pure NO_2 pulsed into the reactor that, as soon as it comes into contact in the air already present, reaches the chemical equilibrium between NO and NO_2, In this way all the photocatalytic tests have been made using a mixture of NO and NO_2 in air. Two initial concentrations of NO_x in the reactor were tested: 1000 ppb in order to follow the same pollutant concentration requested by the ISO 22197-1 rules [15] and 200 ppb that is the alert threshold for NO_x set by the EU Directive 2008/50/CE [10]. Photon sources were provided by a 500 W iron halogenide lamp (Jelosil, model HG 500) emitting in the 320-

400 nm wavelength range (UV-A). The specific UV power on the surface of the samples was 10 Wm^{-2}. The NO_x photocatalytic tests were performed at 30 °C and lasted for 4 h. The actual concentration of pollutants (NO, NO_2 and consequently their sum, i.e. NO_x) in the reactor was determined directly by chemiluminescence (Teledyne, Mod. 200E).

In addition to the kinetics tests of photocatalytic degradation, proper runs were carried out by irradiating the reactor without samples of titanium dioxide inside, to evaluate the effect of the simple photolysis action; after 6 h a maximum total conversion of 3% was obtained and then this contribute will be considered as negligible in this paper. Moreover dark experiments (i.e. with the catalyst inside the reactor but without UV irradiation) were conducted in order to obtain a proper estimation of the NOx adsorption on the different catalytic samples.

The regression of the kinetic parameters of the kinetic model was obtained by the software MATLAB, version 6.6.0.88 release 12 by "The Mathworks, Inc".

3. Results and Discussion

3.1. Textural, structural and morphological characterization

XRD patterns (Fig. 1) show that all the samples are pure anatase, except for P25, which exhibits the well-known phase composition 75:25 in anatase/rutile ratio. The main diffraction peak at about $2\theta = 25.5°$ related to the planes (101) has been employed to calculate the average crystallite sizes (Table 1, third column). Crystallite sizes of A, B and E samples confirm their micro-sized nature and this is reflected in the surface areas that are about 11-12 $m^2\ g^{-1}$ (Table 1, fourth column). Sample C shows lower crystallite size (40

nm) and this is reflected in a higher surface area (23 m^2 g^{-1}). As expected, P25 is a nano-sized powder, being the crystallite size lower than 30 nm.

For D sample Scherrer calculation was not performed, as TEM analysis reveals the presence of both micro-sized and ultrafine fractions (see the following paragraph and Fig. 2 – section d).

TEM images, reported in Figure 2, totally confirm the average crystallite sizes extrapolated by XRD analysis, also excluding the presence of ultrafine particles for all samples except for D. Inspecting in more detail the morphological characteristics of the various samples, it can be evidenced that the reference P25 powder is made up of well-crystallized particles of rather roundish shape, closely packed and with an average size of 20-30 nm. At higher magnification (see the inset to section a of figure 2), it can be evidenced that the most exposed crystal planes belong to the (101) family of the anatase polymorph **(**ICDD Anatase file No. 21-1272).

As for what concerns the A, B and E powders, they all exhibit well crystallized particles possessing smooth edges and average diameter size in the 95-180 nm range, with fringes patterns belonging to the anatase polymorph: see sections b and c in Figure 2, referring to samples A and B, respectively (the image relative to sample E, exhibiting almost the same feature of the former ones, has not been added for the sake of brevity). These features agree very well with the indication coming from the XRD analysis. As for what concerns sample D, TEM investigations again confirm that it is composed by a mixture of both micro-sized crystallites and some ultrafine particles: see section d in figure 2. Finally, C sample exhibits average dimensions in the 40-45 nm range.

The surface states of the TiO_2 particles were analyzed by XPS. No significant differences can be appreciated in the Ti 2p region among all the present samples concerning the

binding energies (BE) and the full width at half-maximum (FWHM) values (not reported for sake of brevity). The peak of Ti 2p3/2 is always regular and the BE at about 485.5 ± 0.1 eV compares well with the data for Ti(IV) in TiO_2 materials [16].

Diffuse reflectance UV-Vis spectra (not reported) were elaborated as mentioned in the experimental section to obtain the band-gap values of the samples studied (Table 1, sixth column). The obtained band-gap values do not exhibit large differences among the various samples and fall in the range expected for anatase [17] and it seems not to be influenced by the crystallites size.

FTIR spectra in the ν(OH) spectral range of the samples in air are reported in Figure 3. All the materials exhibit two complex absorption bands, respectively located in the 3000-3450 cm^{-1} range and at $\nu \geq 3600$ cm^{-1}. On the basis of the spectral behavior and of literature data [8], the former envelope can be ascribed to the stretching mode of all H-bonded OH groups present at the surface of the various solids, whereas the latter corresponds to the stretching mode of all Ti-OH species free from hydrogen bonding interactions [18-20].

It is well known that surface hydroxyls are crucial species for the photo-catalytic process [21]. In particular, photo-generated holes react with water molecules adsorbed on semi-conductor surfaces, resulting in the formation of hydroxyl radicals:

$$TiO_2 + h\nu \rightarrow h^+ + e^- \quad (1)$$

$$h^+ + H_2O \rightarrow {}^{\bullet}OH + H^+ \quad (2)$$

The possible photoreactions occurring on the TiO_2 surface during NO_x abatement are well known and published in the literature [22], as reported in the following:

$$NO + 2{}^{\bullet}OH \rightarrow NO_2 + H_2O \quad (3)$$

$$NO_2 + {}^{\bullet}OH \rightarrow NO_3^- + H^+ \quad (4)$$

Comparing the spectra of both P25 and pigmentary TiO_2 in the OH region, it is evident that P25 is characterized by a significant higher amount of hydroxyl species. This is in agreement with the best performances in NO_x abatement of P25 (see next paragraph). However, also the pigmentary TiO_2 show appreciable amounts of OH groups and this justify their rather good performances in the NO_x degradation.

3.2. Photo-degradation of NO_x

As already mentioned, two initial concentrations of NOx in the reactor were tested: 1000 ppb (to follow the ISO 22197-1 rule, [6]) and 200 ppb (the first alert threshold for NO_2 set by the EU Directive 2008/50/CE). In Table 2 the results obtained with all the catalysts starting from 1000 ppb of NO_x are reported. It is well evident that all the samples show good photocatalytic performances. In particular, after 30 min of reaction the NO_x conversion of B, C, D and E samples is in the range 50-70%. The conversion for the nano-sized P25 is at about 72%. The A sample seems to be more active than P25, showing a conversion close to 80%. After 1h, the NO_x conversion of A, C, D and E samples is higher than 80%. In particular, A and E samples show conversion very close to that of P25 (90%). Only the conversion exhibited by B sample is lower (70%). After 2h the pigmentary samples, with the exception of B sample, reach conversion percentages higher than 90%, P25 reaches the complete conversion. Thus, even if the nano-sized material shows the best performances, as expected also on the basis of FT-IR spectrum in the OH region (Fig. 3), the photo-catalytic activities of the pigmentary samples are very good, in agreement with the presence of appreciable amount of surface hydroxyls.

The results obtained using 200 ppb (Figure 4) are really interesting. As a matter of fact, nano-sized and micro-sized powders show quite the same photocatalytic activity, reaching the complete NO_x degradation within 50 min. Working in more diluted initial

concentrations, the difference between micro and nano samples is highly limited and this means that the amount of surface OH species on the pigmentary TiO_2 is enough to guarantee performances similar to that of P25. The modelistic interpretation of this results is presented in the following paragraph.

2.3. Kinetic model

The photocatalytic system here discussed is characterized by an irreversible adsorption of the final products of the reaction, i.e. the nitrate ions that are produced by the mechanism detailed above [Eq.n (3) and (4)]. These products can be considered adsorbed on the catalyst surface in a absolutely irreversible way; the only way to remove these products in fact is a water washing procedure, obviously not present in our experimental system. It is well known that photocatalytic heterogeneous reactions take place following the Langmuir-Hinshelwood mechanism [11] where only the reactant molecules previously adsorbed on the catalytic surface can take part to the reaction. The kinetic model we propose for the right description of the photocatalytic degradation of NO_x has been written starting from these two aspects. The model takes into account the adsorption and the kinetic photodegradation of both the adsorbed NO and NO_2 species because by considering only their sum (NO_x) it is not possible a detailed description of the system. The differential equations that describe the model are then the following:

$$\frac{dn_{NO_2}}{dt} = -k_{NO2,oss} * \left(\frac{K_{ads,NO_2} * n_{NO_2}}{1 + K_{ads,NO_2} * n_{NO_2} + K_{ads,NO} * n_{NO} + K_{ads,NO_3^-} * n_{NO_3^-}} \right)$$

$$\frac{dn_{NO}}{dt} = -k_{NO,oss} * \left(\frac{K_{ads,NO} * n_{NO}}{1 + K_{ads,NO_2} * n_{NO_2} + K_{ads,NO} * n_{NO} + K_{ads,NO_3^-} * n_{NO_3^-}} \right)$$

where $K_{ads,i}$ (mol^{-1}) are the adsorption constants for the component i and $k_{i,oss}$($mol*min^{-1}$) are the pseudo-first order reaction constant for the component i. All these constants (adsorption and kinetic) might be considered as model's parameters and simultaneously fitted from the experimental data. Nevertheless this approach, in our opinion, is not the right one because the number of parameters is too high to give physical meaning to the same model. A more correct way to operate is to fit in a independent way the adsorption constants and successively to fit the kinetic constants inserting the value of K_{ads} previously obtained. The experimental data used for the first adsorption fitting are those of the runs performed in dark conditions, while obviously the data for the kinetic constants fitting correspond to the UV irradiated runs. This approach for the independent determination of adsorption and kinetic constants in a LH based model has been already used and encouraged by Gmehling et al [23]. The adsorption of NO_x has been modeled using the following equation:

$$-\frac{d(NO_x)bulk}{dt} = k_{ads} * n_{(NO_x)bulk} - k_{des} * n_{(NO_x)ads}$$

Where NOx stands for either NO and NO_2 and with

$$K_{ads} = \frac{k_{ads}}{k_{des}}$$

The results of the adsorption experiments for P25 and sample A are reported in Fig. 5 together with the predicted courses obtained with the independent regressed constants, that are reported in Table 3. The adsorption constant (K_{ads}) for NO_3^- was set to $2*10^6$ because these species are irreversibly adsorbed on the catalysts. The irreversible adsorption of the nitrate and nitrite species is well known in the scientific literature [24, 25] and for this reason it was chosen such a high numerical value.

For the samples A-E similar K_{ads} values for both the NOx species were obtained and for this reason average adsorption constants were used for all the studied catalysts. The fitting procedure for the achievement of constant kinetics was made using all the experimental kinetic data and using the adsorption constants before determined. The experimental values and the predicted course are reported in Fig 6 for P25 sample and Fig. 7 a and b for P25 and A samples, respectively (NOx starting concentration equal to 1000 for Fig. 6 and 200 ppb for Fig. 7 a-b). The numerical values of the obtained kinetic constants are reported in Table 3. An higher adsorption constant value was obtained for samples A-E compared to the one obtained for P25. This is due to the different characteristics of the sample, in particular to the fact that the latter is nano-sized while the others are micrometric. The calculated curves are very near for both the initial tested concentrations and this seems to validate the proposed model. An attempt to fitting the adsorption and kinetic constant to kinetic data only resulted in very small residual errors, but also in a very poor extrapolability of the model to experimental data not included in the fitting procedure.

This model (together with the numerical values of the adsorption and kinetic constants) justify the experimental evidence for which nano and micro samples give very similar NOx degradation at low pollutant concentrations.

4. Conclusions

In this work, five commercial pigmentary powdered TiO_2 were characterized and their photo-catalytic performances in NO_x degradation were compared to that of P25 nano-powder that is specifically sold as photocatalyst and worldwide used as photocatalyst reference material. Band gap values fall in the classical range (3.15-3.28 eV) of the anatase polymorph and without any particular difference due to the different crystallites size

notwithstanding, the tested samples size ranges from 40 (or even less in sample D) to 180 nm.

The photocatalytic activity in NO_x degradation was tested with a concentration of 1000 ppb (to follow the 22197-1 ISO rules) and 200 ppb (2008/50/CE threshold alert). As expected, at 1000 ppb P25 shows the highest efficiency, reaching the complete pollutant degradation only after 120 min; however, pigmentary powders exhibit very good efficiency, reaching conversion percentages higher than 90%. At 200 ppb of NO_x nano-sized and micro-sized powders show quite the same photocatalytic activity.

The presence of surface OH groups, which are well known to play a key role in leading to a good photocatalytic activity, was assessed by FTIR spectroscopy. It was evident that P25 is characterized by a significant higher amount of hydroxyl species, in agreement with the best performances in NO_x abatement at 1000 ppb. However, also the pigmentary TiO_2 show appreciable amounts of OH groups and this justify their good catalytic performances at 1000 ppb and the same activity of P25 at 200 ppb. A detailed LH model working on the hypothesis that the products of the reaction are irreversibly adsorbed on the catalyst surface, justify the experimental results. The adsorption and kinetic constants involved in this model were fitted in a independent way, to improve the physical consistence of the model.

As matter of fact, this work shows that all samples reveal good photoactivity in the photodegradation of NO_x in gas phase with an evident superiority of the nano-sized sample. However, the gap of activity between nano and micro-sized samples tends to be avoided when the starting NO_x concentration was reduced and fixed from 1000 to 200 ppb, a precise amount that is the first alert threshold for NO_x in air (World Health Organization). These are really important results, that suggest the possibility to replace

nano powders with micro-sized TiO_2, being these nano-photocatalysts potentially dangerous due to the risk towards the human safety.

References

[1] D. P. Macwan, P. N. Dave, S. Chaturvedi, A review on nano-Ti02 sol—gel type syntheses and its applications, Mater. Sci. 46 (2011) 3669-3686.

[2] C. Morterra, V. Bolis, E. Fisicaro, The hydrated layer and the adsorption of carbon monoxide at the surface of titania (anatase), Colloids and Surfaces 41 (1989) 177–188.

[3] D. Beydoun, R. Amal, G. Low, S. McEvoy, Role of nanoparticles in photocatalysis, J. Nanopart Res. 1 (1999) 439-458.

[4] A. Di Paola, E. García-López, G. Marcì, L. Palmisano, A survey of photocatalytic materials for environmental remediation, J. Haz. Mat. 211– 212 (2012) 3– 29.

[5] A. Quigg, W.-C. Chin, C.-S. Chen, S. Zhang, Y. Jiang, A.-J. Miao, K.A. Schwehr, C. Xu, P.H. Santschi, Direct and Indirect Toxic Effects of Engineered Nanoparticles on Algae: Role of Natural Organic Matter, ACS Sust. Chem. & Eng. 1 (2013) 686−702.

[6] C. L. Bianchi, C. Pirola, S. Gatto, S. Nucci, A. Minguzzi, G. Cerrato, S. Biella, V. Capucci, New surface properties in porcelain gres tiles with a look to human and environmental safety, Adv. in Mat. Sci. and Eng. Volume 2012, Article ID 970182, 8 pages.

[7] C. L. Bianchi, S. Gatto, C. Pirola, M. Scavini, S. Vitali, V. Capucci, Micto-TiO_2 as a starting material for new photocatalytic tiles, Cem. Con. Comp. 36 (2013) 116-120.

[8] C. L. Bianchi, S. Gatto, C. Pirola, A. Naldoni, A. Di Michele, G. Cerrato, V. Crocellà, V. Capucci, Photocatalytic degradation of acetone, acetaldehyde and toluene in gas-phase: comparison between nano and micro-sized TiO2, Appl Catal B: Environmental, 146 (2014) 123-130.

[9] http://www.who.int/en/

[10] http://eur-lex.europa.eu/LexUriServ/LexUriServ.do?uri=OJ:L:2008:152:0001:0044:EN:PDF

[11] C. S. Turchi, D. F. Ollis, Photocatalytic degradation of organic contaminants: mechanisms involving hydroxyl radaical attack, J. Catal. 122 (1990) 178-192.

[12] G. Kortüm, Reflectance Spectroscopy, Springer-Verlag, Berlin, 1969.

[13] S. Ardizzone, C. L. Bianchi, G. Cappelletti, A. Naldoni, C. Pirola, Photocatalytic degradation of toluene in gas phase: relationship between surface species and catalyst features, Environmental Sci. & Technol. 42 (2008) 6671–6676.

[14] C. L. Bianchi, C. Pirola, E. Selli, S. Biella, Photocatalytic NOx abatement: the role of the material supporting the TiO2 active layer, J. Hazardous Mat. 211-212 (2012) 203-207.

[15] www.iso.org

[16] G. Cappelletti, C.L. Bianchi, S. Ardizzone, XPS study of the surfactant film adsorbed onto growing titania nanoparticles, Appl. Surf. Sci. 253 (2006) 519-524.

[17] U. Diebold, The surface science of titanium dioxide, Surf. Sci. Rep. 48 (2003) 53-229.

[18] L.H. Little, Infrared Spectra of Adsorbed Species, Academic Press, London, 1966.

[19] C. Morterra, An infrared spectroscopic study of anatase properties. 6. Surface hydratation and strong Lewis acidity of pure and sulfate-doped preparations, Faraday Transactions 1 84 (1988) 1617–1637.

[20] C. Morterra, V. Bolis, E. Fisicaro, The hydrated layer and the adsorption of carbon monoxide at the surface of titania (anatase), Colloids and Surfaces 41 (1989) 177–188.

[21] J. Angelo, L. Andrade, L. M. Madeira, A. Mendes, An overview of photocatalysis phenomena applied to NOx abatement, J. Environ. Manag. 129 (2013) 522-539

[22] C. Guo, X. Wu, M. Yan, Q. Dong, S. Yin, T. Sato, S. Liu, The visible-light driven photocatalytic destruction of NOx using mesoporous TiO2 spheres synthesized via a “water-controlled release process”, Nanoscale 5 (2013) 8184-8191.

[23] T. Popken, L. Gotze, J. Gmehling, Reaction kinetics and chemical equilibrium of homogeneously and heterogeneously catalyzed acetic acid esterification with methanol and methyl acetate hydrolysis, Ind. Eng. Chem. Res. 39 (2000) 2601-2611.

[24] T. Martinez, A. Bertron, E. Ringot, G. Escadeillas, Degradation of NO using photocatalytic coatings applied to different substrates, Building and Environment 46 (2011) 1808-1816.

[25] S. Laufs, G. Burgeth, W. Duttlinger, R. Kurtenbach, M. Maban, C. Thomas, P. Wiesen, J. Kleffmann, Conversion of nitrogen oxides on commercial photocatalytic dispersion paints, Atmos. Environ. 44 (2010) 2341-2349.

Table 1. Main features of the TiO_2 samples.

Sample	anatase: rutile	Average crystallite size (nm)	SSA (m^2/g)	XPS	Band gap (eV)
P25	75:25	26	50	Ti(IV)	3.21
A	100	105	12	Ti(IV)	3.15
B	100	95	11	Ti(IV)	3.25
C	100	40	23	Ti(IV)	3.28
D	100	Mix (micro-sized + ultrafine)	11	Ti(IV)	3.25
E	100	180	11	Ti(IV)	3.17

Table 2. Photocatalytic activity in the degradation of NO_x (1000 ppb).

Sample	Conv. NO_x % after 30'	Conv. NO_x % after 60'	Conv. NO_x % after 120'
P25	72	90	99
A	79	89	92
B	52	70	84
C	62	81	93
D	62	83	92
E	67	88	97

Table 3. NO and NO_2 adsorption and kinetic constants

Sample	$\mathbf{K_{ads,NO_2}}$ **[mol^{-1}]**	$\mathbf{K_{ads,NO}}$ **[mol^{-1}]**	$\mathbf{k_{,NO_2}}$ **[mol*min^{-1}]**	$\mathbf{k_{,NO}}$ **[mol*min^{-1}]**
P25	0.42	0.05	0.99	0.39
A	0.73[a]	0.29[a]	0.30	0.12
B	0.73[a]	0.29[a]	0.16	0.18
C	0.73[a]	0.29[a]	0.15	0.11
D	0.73[a]	0.29[a]	0.14	0.15
E	0.73[a]	0.29[a]	0.17	0.15

a: averaged values for all the micrometric samples (A, B, C, D, E). The regression procedure gave very close values for these ones ($0.73 \pm 0.03; 0.29 \pm 0.02$) and for this reason the authors chose to report an average result (by which the difference between experimental and calculated is always very low)

Figure captions

Figure 1: XRD patterns of the studied samples.

Figure 2: TEM images of the various TiO_2 powders. Section a: reference P25; Section b: A powder; Section c: B powder; Section d: D powder.

Figure 3: FT-IR spectra of the samples in air.

Figure 4: NO_x photodegradation starting from 200 ppb, room T, RH: 40%, UV-A irradiation with the samples: A (▲), B (■), P25 (♦).

Figure 5: NOx dark runs (adsorption kinetics), experimental values: full points for P25 for NO (■) and NO_2 (▲); empty points for sample A for NO (□) and NO_2 (Δ). The corresponding curves are the calculated ones with the adsorption constants fitted and reported in Table 3.

Figure 6: NOx photodegradation with P25 sample: 1000 ppb, room T, RH:40% UV-A irradiation: experimental values for NO (■) and NO_2 (▲). The corresponding curves are the calculated ones from the kinetic model.

Figure 7: NOx photodegradation: 200 ppb, room T, RH:40% UV-A irradiation of sample a) P25, b) A. Experimental values for NO (■) and NO_2 (▲). The corresponding curves are the calculated ones from the kinetic model.

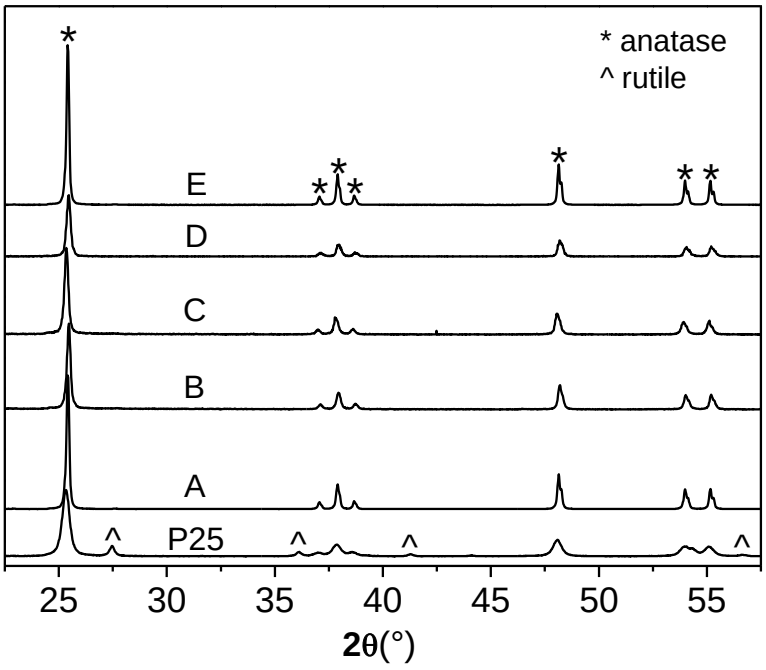

Figure 1

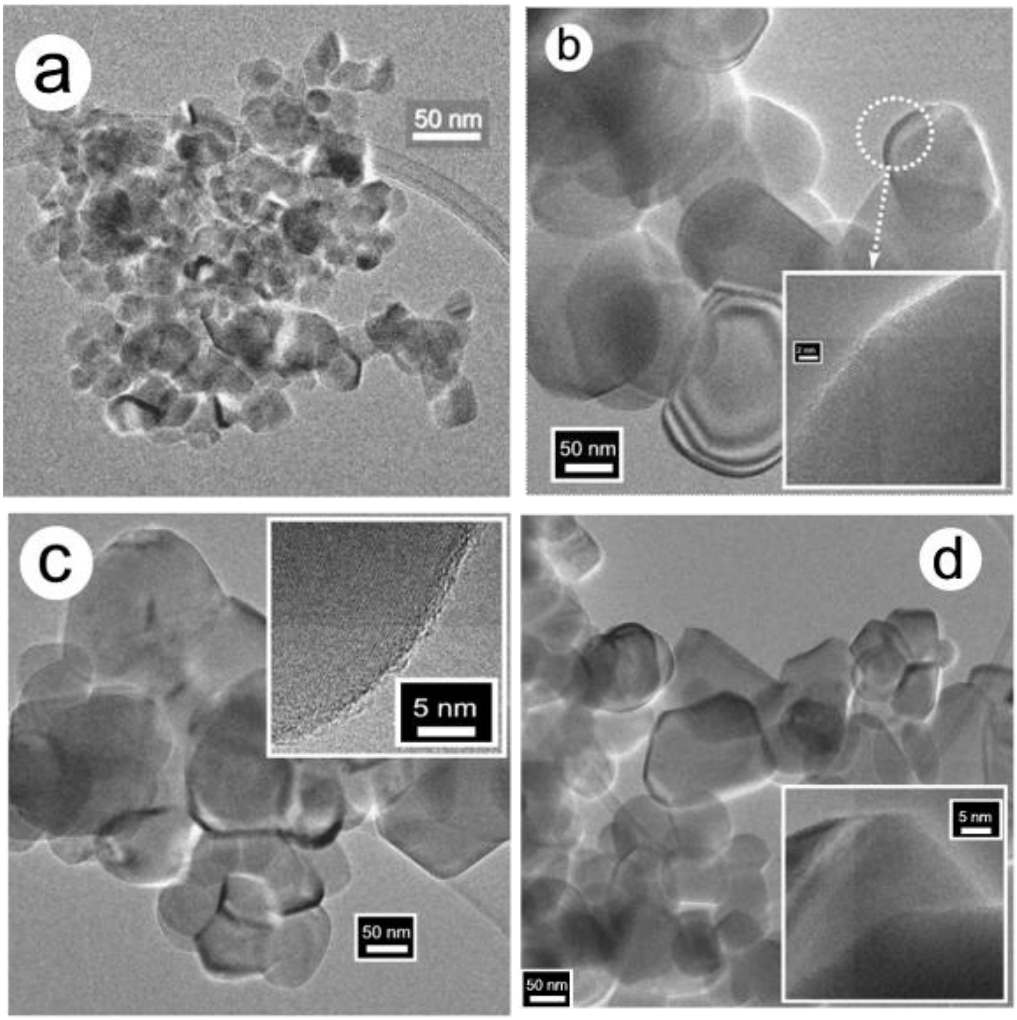

Figure 2.

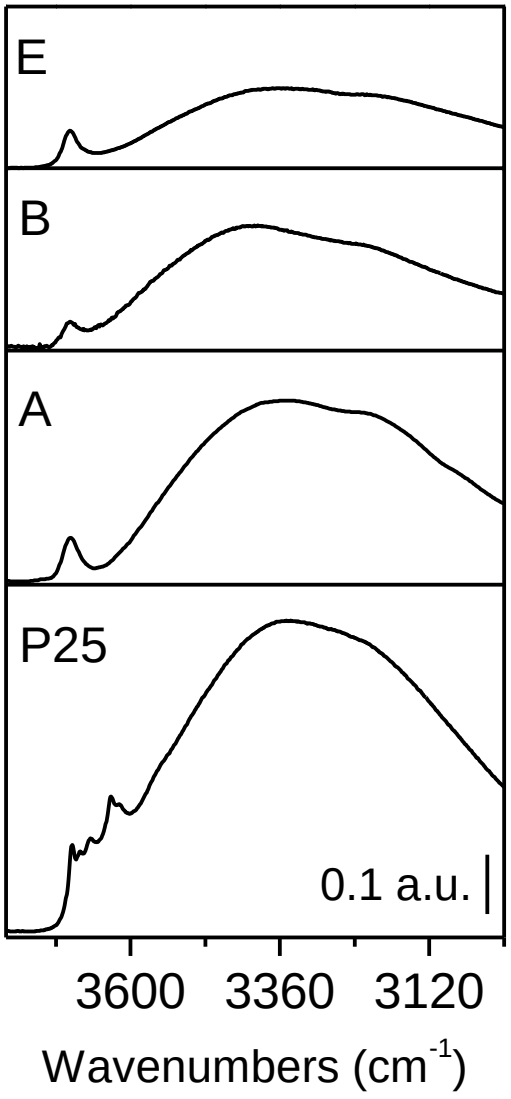

Figure 3

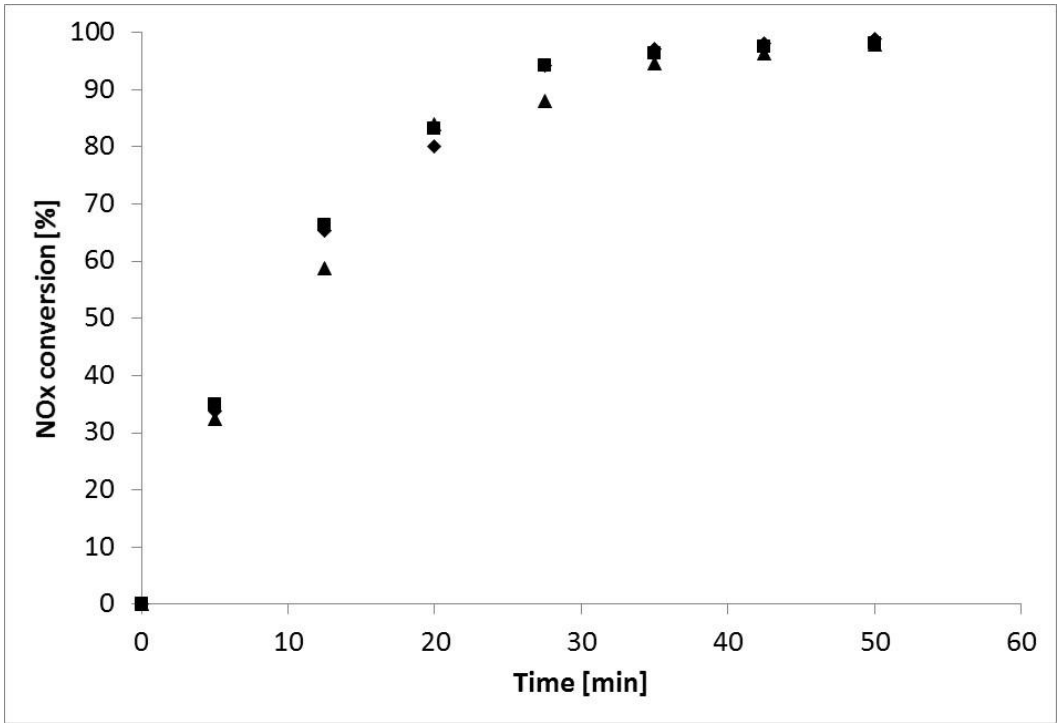
NOx conversion [%]
100
90
80
70
60
50
40
30
20
10
0
0
10
20
30
40
50
60
Time [min]

Figure 4

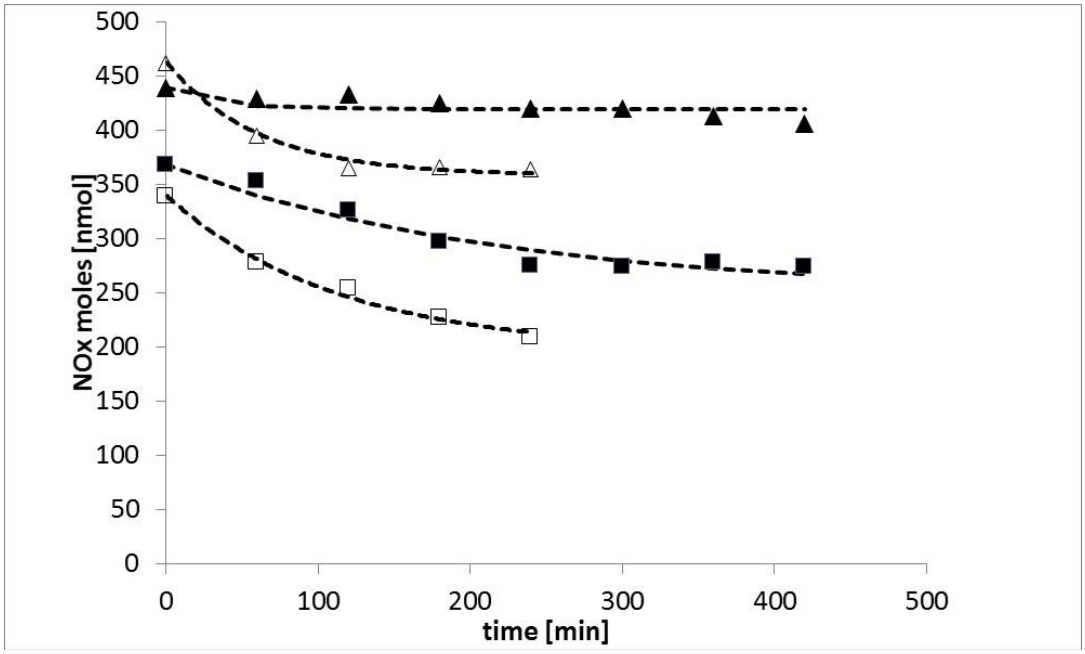
500
450
400
350
300
250
200
150
100
50
0
NOx moles [nmol]
0
100
200
300
400
500
time [min]

Figure 5

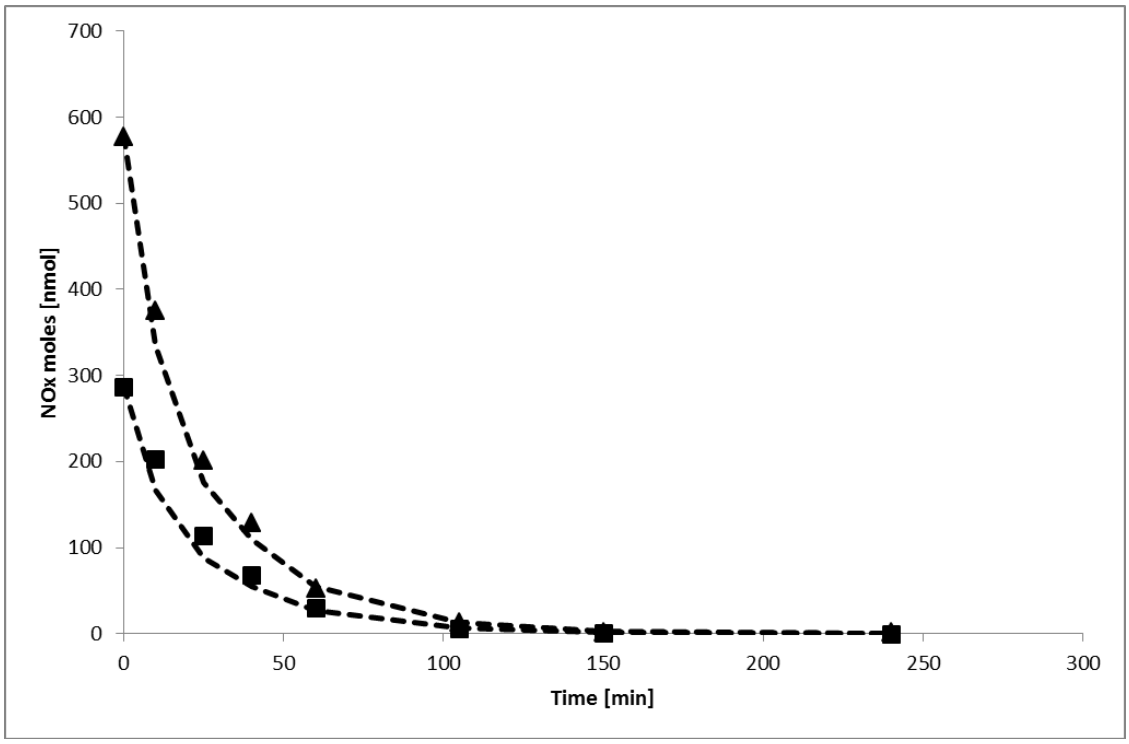
700
600
500
400
300
200
100
0
NOx moles [nmol]
0
50
100
150
200
250
300
Time [min]
Figure 6

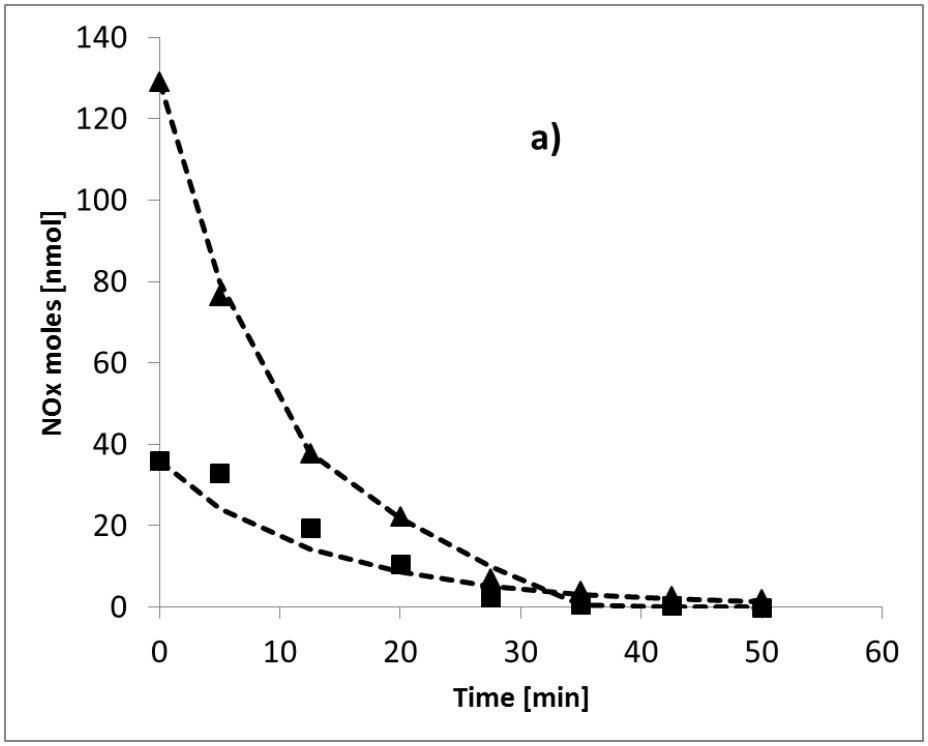

Figure 7a

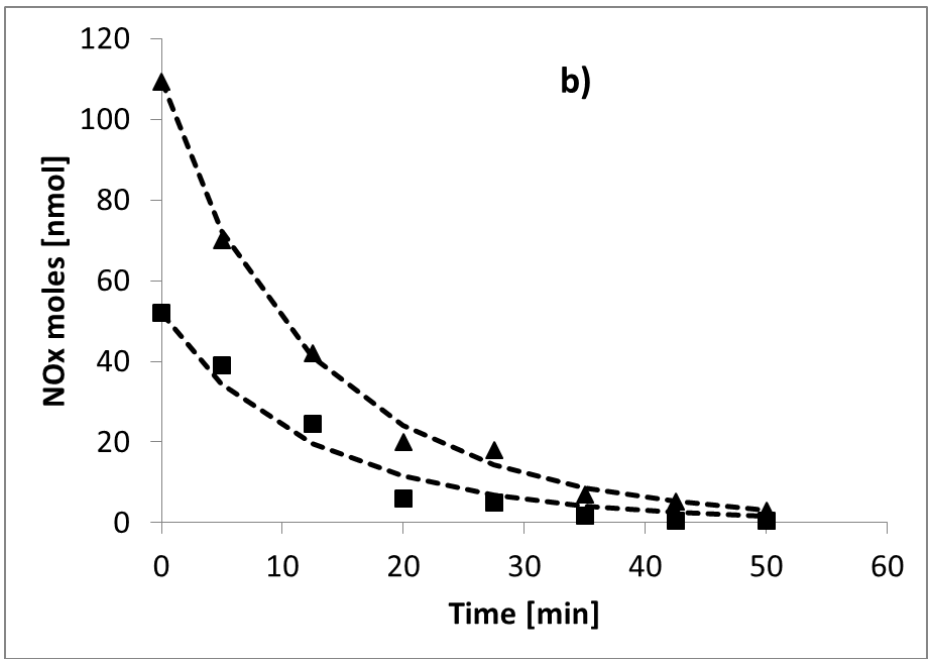

Figure 7b

Figure 7